Temporal variability of near-bottom dissolved oxygen during upwelling off central Oregon

Citation	Adams, K. A., J. A. Barth, and F. Chan (2013), Temporal variability of near-bottom dissolved oxygen during upwelling off central Oregon, Journal of Geophysical Research: Oceans, 118, doi:10.1002/jgrc.20361.
DOI	10.1002/jgrc.20361
Publisher	American Geophysical Union
Version	Version of Record
Terms of Use	http://cdss.library.oregonstate.edu/sa-termsofuse

JOURNAL OF GEOPHYSICAL RESEARCH: OCEANS, VOL. 118, 4839–4854, doi:10.1002/jgrc.20361, 2013

Temporal variability of near-bottom dissolved oxygen during upwelling off central Oregon

Katherine A. Adams,[1] John A. Barth,[1] and Francis Chan[2]

Received 21 November 2012; revised 9 July 2013; accepted 18 August 2013; published 2 October 2013.

[1] In the productive central-Oregon coastal upwelling environment, wind-driven upwelling, tides, and topographic effects vary across the shelf, setting the stage for varied biogeochemical responses to physical drivers. Current, temperature, salinity, and dissolved oxygen (DO) measurements from three moorings deployed during the upwelling seasons of 2009–2011 off the central-Oregon coast are analyzed over three time bands (interannual, subtidal, tidal) to explore the relationship between mid (70 m) and inner-shelf (15 m) upwelling dynamics and the associated effect on DO. Topographic effects are observed in each time band due to the Heceta and Stonewall Bank complex. Seasonal cumulative hypoxia (DO < 1.4 mL L^{-1}) calculations identify two regions, a well-ventilated inner shelf and a midshelf vulnerable to hypoxia (98 ± 15 days annually). On tidal timescales, along-shelf diurnal (K1) velocities are intensified over the Bank, 0.08 m s^{-1} compared with 0.03 m s^{-1} to the north. Interannual variability in the timing of spring and fall transitions, defined using glider-measured continental slope source water temperature, is observed on the midshelf. Interannual source water DO concentrations vary on the order of 0.1 mL L^{-1}. Each spring and summer, DO decline rates are modulated by physical and biological processes. The net observed decrease is about 30% of the expected draw down due to water-column respiration. Physical processes initiate low-oxygen conditions on the shelf through coastal upwelling and subsequently prevent the system via advection and mixing from reaching the potential anoxic levels anticipated from respiration rates alone.

Citation: Adams, K. A., J. A. Barth, and F. Chan (2013), Temporal variability of near-bottom dissolved oxygen during upwelling off central Oregon, *J. Geophys. Res. Oceans*, *118*, 4839–4854, doi:10.1002/jgrc.20361.

1. Introduction

[2] Dissolved oxygen concentrations of continental shelf waters are modulated by physical and biological processes. Wind-driven coastal upwelling currents bring cold, salty, oxygen-poor, and nutrient-rich waters onto the Oregon shelf each spring and summer, commencing with the spring transition [*Huyer et al*., 1979]. The delivery of nutrients via onshore flow of upwelled source water fuels photic-zone productivity and subsequent subsurface microbial respiration over the shelf. The relative contribution of processes, such as wind-driven advection and microbial respiration, to oxygen variability on the shelf is unknown. Here, we relate continuous time series of near-bottom dissolved oxygen (DO) concentrations to forcing mechanisms across the Oregon shelf and across time bands to identify drivers of oxygen variability. Understanding the drivers of DO spatio-temporal variability is a critical step to understanding the past and predicting the future of low-oxygen events on the Oregon shelf.

[3] Dissolved oxygen (DO) concentrations on the Oregon shelf range between high, ventilated values during winter (>6 mL L^{-1}, 260 μmol kg^{-1}) and minimum values during the summertime upwelling season (<2 mL L^{-1}, 87 μmol kg^{-1}) [*Pierce et al*., 2012]. Recently, oxygen minimum values on the Oregon shelf have fallen below the hypoxic threshold (<1.4 mL L^{-1}, 60 μmol kg^{-1}) [*Chan et al*., 2008]. Recent observational studies of DO variability along the western coast of the U.S. reveal changes occurring over several decades based on ship or, more recently, glider measurements. These long-term studies show a significant decline in DO concentration and a shoaling of the hypoxic boundary over a span of 50 years in the eastern subarctic Pacific [*Whitney et al*., 2007] and the continental shelf waters off Oregon [*Pierce et al*., 2012] and California [*Bograd et al*., 2008]. Less is known about dissolved oxygen variability and its response to mechanisms on shorter time scales over the Oregon shelf as the temporal resolution of previous studies do not allow for subseasonal scale analysis. Along the California Current system, known drivers

[1]College of Earth, Ocean and Atmospheric Sciences, Oregon State University, Corvallis, Oregon, USA.
[2]Department of Zoology, Oregon State University, Corvallis, Oregon, USA.

Corresponding author: K. A. Adams, College of Earth, Ocean and Atmospheric Sciences, Oregon State University, 104 CEOAS Admin. Bldg., Corvallis, OR 97331, USA. (kadams@coas.oregonstate.edu)

2169-9275/13/10.1002/jgrc.20361

of DO temporal variability on shorter timescales than decadal include advective currents and biochemical consumption [*Connolly et al*., 2010; Washington], shelf width [*Send and Nam*, 2012; Southern California], and El Niño/Southern Oscillation (ENSO) [*Nam et al*., 2011; Southern California].

[4] The response to upwelling along the Oregon shelf varies with alongshelf bottom topography [*Castelao and Barth*, 2005; *Barth et al*., 2005]. In a region of complex bottom topography, such as the submarine Heceta and Stonewall Bank Complex (HSBC) (44–44.25°N, Figure 1), a 3-D flow regime has been established indicating an intermittent recirculation around the Bank [*Barth et al*., 2005]. In the along-shelf direction, the coastal upwelling jet (0.25–0.50 m s^{-1}) is deflected offshore due to the geometry of the Bank. On the lee, or onshore, side of the Bank, a high chlorophyll signal coincident with weak currents has been observed [*Barth et al*., 2005]. Here, we expand on this finding by relating upwelling and dissolved oxygen dynamics at locations on the mid and inner shelf, over and north of the Bank (44.25°N).

[5] Biological responses to low-oxygen waters vary by species and oxygen concentration [*Gray et al*., 2002; *Diaz and Rosenberg*, 1995]. Typical low DO water categorizations include hypoxic (1.4 mL L^{-1}), severely hypoxic (0.5 mL L^{-1}) or anoxic (0 mL L^{-1}). Although long-term biological effects are largely unknown, low-oxygen events have devastating immediate effects on biological communities as evidenced off Oregon by the unprecedented crab mortalities in 2002 [*Grantham et al*., 2004] and shelf anoxia observed in 2006 [*Chan et al*., 2008]. Hypoxia has become more frequent since the early 2000s on the central Oregon shelf [*Chan et al*., 2008], although with high temporal variability and to varying degrees of severity. With continuous time series data, we quantify the exposure to hypoxia on local biological communities not yet reported due to the coarse temporal resolution of previous observational studies. Additionally, bottle respiration rate data are presented from the Oregon midshelf to quantify the contribution of biological processes on low-oxygen events.

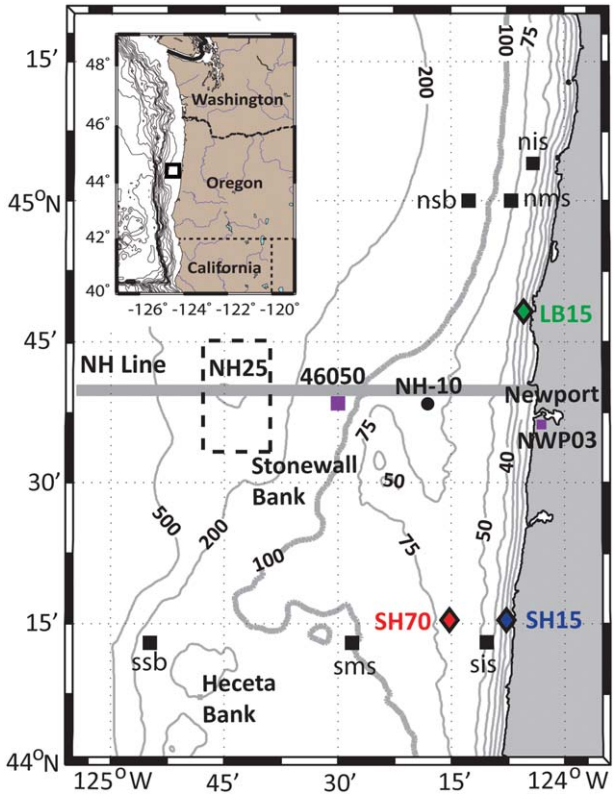

Figure 1. Central-Oregon shelf study area with Pacific northwestern U.S. inset. Mooring locations from COAST (2001; black squares), NH-10 (2009), PISCO (2009–2011; SH15 and LB15), and MI_LOCO (2009–2011; SH70). Wind measurements from NDBC 46050 and NWP03, as well as glider measurements from Newport-hydrographic line (NH) station NH-25 (dashed box) are also shown.

[6] In this paper, we investigate the variability in dissolved oxygen concentrations along the inner and midshelf areas of the central Oregon coast and estimate the relative importance of physical and biological drivers. Continuous moored time series collected from three consecutive upwelling seasons (2009–2011) off the central Oregon midshelf (44.25°N, 70 m isobath) and inner shelf (44.25°N and 44.75°N, 15 m isobath) (see Figure 1) are analyzed in three time bands: subtidal, tidal, and interannual. In section 2, we present data sources and processing methods. In section 3, results from investigating drivers of oxygen variability at each time band through correlation analysis, harmonic regression analysis, and oxygen decline analysis are presented. Section 4 contains a discussion explaining the results within the context of previous findings and theories. We conclude and identify future research in section 5.

2. Data Sources and Processing

2.1. Data Sources

[7] The mooring component of the MI_LOCO (Microbial Initiative in Low-Oxygen areas off Concepción and Oregon) Oregon State University (OSU) program focused on collecting near-bottom data from the 70 m isobath off Strawberry Hill (SH70; 44.25°N, 124.25°W), near Yachats, Oregon (Figure 1), during the upwelling seasons of 2009 and 2010. An additional year of sampling was conducted in 2011 with partial support of the MI_LOCO program. Three deployments were conducted each season with turnarounds ranging from 2 to 9 days (Figure 2). Instruments measuring temperature, conductivity, dissolved oxygen (DO), and currents were attached to an all-aluminum frame on platforms approximately 0.5 m above the ocean floor. Sea-Bird Electronics, Inc. SBE16plus CTD (conductivity, temperature, depth) and SBE43 (DO) sensors collected measurements on 30 min intervals. Current measurements were made using a Teledyne RD Instruments 300 kHz Workhorse Sentinel Acoustic Doppler Current Profiler (ADCP) on 5 min sampling intervals.

[8] CTD and DO sensors were factory calibrated before and after each field season. ADCP instruments passed all predeployment tests including internal compass calibration for hard and soft iron corrections for each deployment. Mooring data were field calibrated using the weekly-biweekly MI_LOCO ship-based CTD+DO program cast data from the SH70 site (F. Chan, unpublished data, 2013). Calibration casts were also performed on the DO sensor at

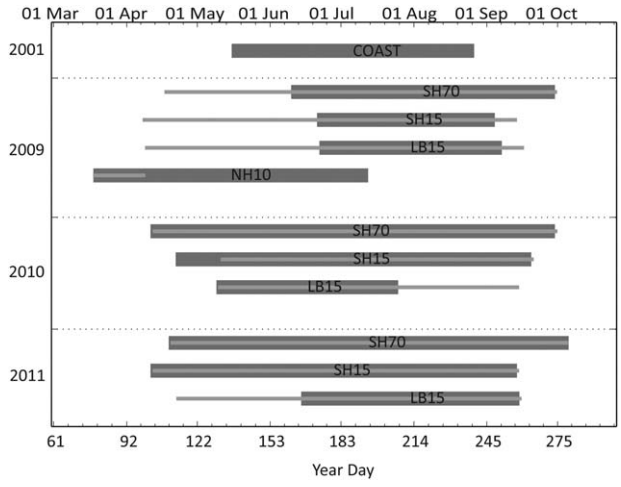

Figure 2. Timeline of CTD (thin) and ADCP (thick) measurements from COAST, SH15, LB15, SH70, and NH-10 mooring programs for indicated years.

the end of each deployment. During a calibration cast, the moored CTD+DO instrument is attached to a profiling instrument (Sea-Bird Electronics, Inc. SBE25 with SBE43) and data are collected for 5 min at 5, 25, and 50 m water depths. The profiling DO sensor is calibrated periodically through in-laboratory Winkler titrations of water samples taken throughout the field season. Data from calibration casts were plotted against each other to determine inaccuracies in the moored instrument measurements, e.g., drift. Based on analysis of field calibrations, all factory calibration constants for the moored DO sensor were proven accurate throughout the field season with little to no observed drift between annual factory calibrations.

[9] Since 1998, the Partnership for Interdisciplinary Studies of the Coastal Ocean (PISCO) program at OSU has maintained inner-shelf moorings along the 15 m isobath during the upwelling season along the central Oregon coast. *Kirincich and Barth* [2009] analyzed physical data from the 2004 season. During the 2009–2011 field seasons, observations at the Lincoln Beach (LB15, 44.8°N) and Strawberry Hill (SH15, 44.25°N) locations were maintained from April to September (Figure 2). Each mooring was outfitted with a Teledyne RD Instruments 600 kHz Workhorse Sentinel ADCP sampling at 2 min intervals, a Sea-Bird Electronics, Inc. SBE16plus CTD and SBE43 DO sensor both with a 15 min sampling interval. Calibration of instruments on the LB15 and SH15 moorings is similar to the SH70 (MI_LOCO) mooring calibration.

[10] Scalar and current data collected in 2009 from 10 miles offshore on the Newport Hydrographic Line (NH10, 44.6°N; Figure 1) are included in this analysis (Figure 2). Data from NH10 are available through the NDBC program as station 46094: http://www.ndbc.noaa.gov. Temperature, salinity, and dissolved oxygen measurements were made at a depth of 73 m in 80 m of water by a Sea-Bird Electronics, Inc. SBE16plus with a SBE43. Data were collected on 2 h intervals. Scalar data from this location are used to extend the SH70 midshelf mooring record of 2009 before year day 100 (Figure 2) in order to capture the spring transition. Current records at this location, measured by a downward-looking Teledyne RD Instruments 300 kHz ADCP, cover approximately 8–65 m of the water column.

[11] Current data from the Coastal Ocean Advances in Shelf Transport (COAST) program in 2001 are included to give context both north and south of the Bank spanning the inner shelf, midshelf, and shelf break (Figures 1 and 2) [*Boyd et al*., 2002].

[12] Hourly averaged wind speed and direction are from the National Data Buoy Center (NDBC) buoy 46050 (44.64° N, 124.53°W) (Figure 1). *Kirincich et al*. [2005] calculated the correlation between meteorological wind stations off and on shore and found winds at buoy 46050 to be strongly correlated to the winds on the coast (>0.87 correlation coefficient). North-south and east-west components of wind stress were calculated per *Large et al*. [1994]. Ordinal directions were used rather than principal axis directions (Table 1). Gaps in the 2011 NDBC 46050 record were filled by applying regression coefficients (slope = 0.90, offset = −0.34 ms^{-1}) to the onshore C-MAN station NWP03 (44.61°N, 124.07°W) wind data. The correlation coefficient between the measured north-south velocity at 46050 and NWP03 is 0.76 at zero lag with maximum correlation of 0.77 at 1 h lag (offshore 46050 leading onshore NWP03).

[13] Data collected along the Newport Hydrographic line (NH line) by Teledyne Webb Research Slocum gliders, operated by the OSU glider research group, are used as a proxy for upwelling source water. Near-bottom shelf waters originate from water depths between 100 and 200 m off shore during upwelling (σ_t: 26.4–26.6 kg m^{-3}, DO: 1.84–2.30 mL L^{-1}) [*Pierce et al*., 2012]. We define glider-measured source water as $\sigma_t = 26.5 \pm 0.01$ kg m^{-3}, 100–200 m between the 250 and 300 m isobaths, within ± 0.2 degrees of latitude (22

Table 1. Data Source Locations and Principal Axes Rotation Angles for Individual Deployments

	Latitude (°N)	Longitude (°E)	θ (° From N)
SH15			
2009 a,b	44.25	−124.13	7.7, 6.6
2010 a,b			5.3, 8.1
2011 a,b,c			4.9, 2.3, 9.3
LB15			
2009 a,b	44.80	−124.09	20.4, 21.4
2010 a,b			18.8, 14.8
2011 a,b			25.0, 16.5
SH70			
2009 a,b	44.25	−124.25	5.0, −10.1
2010 a,b,c			−3.4, −7.6, 9.9
2011			1.5, −8.0, −5.9
NH10			
2009	44.63	−124.30	18.3
2010			21.4
46050 τ_y			
2009	44.64	−124.50	5.1
2010			2.1
2011			7.7
COAST 2001			
nis	45.07	−124.07	9.4
nms	45.00	−124.12	6.8
nsb	45.00	−124.21	6.9
sis	44.27	−124.17	1.4
sms	44.22	−124.47	13.8
ssb	44.22	−124.91	23.7

km) from the NH line. This region surrounds NH25 (44.65°N 124.65°W, approximately bottom depth 285 m; Figure 1) located 46 km (25 nautical miles) off shore of Newport, Oregon.

[14] At the SH70 station, near-bottom water samples were collected at 10 time points over the course of the upwelling season in 2009 in order to determine water column oxygen utilization rate measurements. Water was collected from depth via large volume (20 L) Niskin bottles and immediately dispensed into duplicate, acid-washed, ground glass stoppered 300 mL borosilicate bottles. Each bottle was equipped with internal polymer-embedded oxygen-sensitive platinum porphyrine fluorophore pigment spots to enable oxygen concentration determination via a lifetime-based oxygen optode system (Presens GmbH, Regensburg, Germany) [*Steindler et al*., 2011]. Briefly, oxygen concentration is calculated from the phase shift between pulsed excitation light and pigment fluorescence [*Tengberg et al*., 2006] as compensated by temperature. This approach enables high-precision determination of oxygen change in individual bottles without breaching the gas-tight seal. The sensor was calibrated precruise with air-saturated (100% DO) and sodium sulfite-enriched (0% DO) bottles. Initial oxygen concentrations were determined within 2–4 hr of collection and bottles were held in a dark on-deck temperature-adjusted water bath until transfer to a temperature-controlled (within 1°C of in-situ temperature) dark incubator in the laboratory. Reference 100 and 0% DO saturation bottles were incubated along side to control for potential sensor drift. Subsequent oxygen concentration readings were taken approximately 18 and 42 h from initial time zero measurements to calculate water column respiration rates (Table 2).

2.2. Data Processing

[15] The 5 min (MI_LOCO) and 2 min (PISCO) current records were averaged to 1 h ensembles. The sea surface was detected using maximum intensity and pressure measurements for the PISCO moorings. Since pressure measurements were not recorded by the MI_LOCO mooring ADCP, beam intensity measurements were used as an indicator of the surface; removal of the closest eight bins to the sea surface and deepest bin sufficiently masked feedback from the ocean surface and bottom. Along and cross-shelf velocity components were derived from the north and east velocity measurements by principal axes rotation. Angles of rotation (Table 1) at LB15 and SH15 agree with previous analysis [*Kirincich et al*., 2005].

[16] Temperature, salinity, and dissolved oxygen records were cleaned for erroneous values and hourly averaged. Density anomaly values, $\sigma_t = \rho(S,T,0) - 1000$, are calculated from CTD-measured temperature and salinity. Scalar and current records for each deployment were low-pass filtered (loess filter with 40 h cutoff window) [*Schlax and Chelton*, 1992], concatenated, and gap-filled using a boundary value solver, Inpaint_nans (J. D'Errico, unpublished data, 2004), available from the MATLAB Central File Exchange: http://www.mathworks.com/matlabcentral/fileexchange/4551. This low-frequency data product is used in the event-scale and interannual analysis (sections 3.1, 3.2, and 3.4). The residual of the raw data and low-frequency data product for a single deployment in 2009 is used for the high-frequency analysis (section 3.3).

[17] For the interannual analysis, we align DO and density time series by spring transition dates, since the onset of upwelling varies between years. We use two methods to

Table 2. Water Column Respiration Rates Measured From Near-Bottom Samples Taken at SH70 in 2009 Are Shown Along With Expected DO (mL L^{-1}) Due to Respiration, Assuming a Constant Average Rate Between Samples and an Initial DO Value of 1.75 mL L^{-1} From 2009 SH70 Oxygen Time Series at Year Day 0 (Figures 8c and 12a)[a]

Year Day 2009	Days of Upwelling	Bottle Respiration Rate 10^{-2} (mL L^{-1} day^{-1})	No. Days	Average Respiration Rate 10^{-2} (mL L^{-1} day^{-1})	Expected Oxygen Due to Respiration (mL L^{-1})
96	0	−1.55[b]			1.75
			9	−1.55	1.61
105	9	−1.55			
			41	−1.52	0.99
146	50	−1.48			
			14	−2.21	0.68
160	64	−2.93			
			28	−2.23	0.05
188	92	−1.54			
			22	−2.82	−0.57
210	114	−4.09			
			6	−4.53	−0.84
216	120	−4.97			
			9	−3.85	−1.18
225	129	−2.73			
			10	−3.37	−1.52
235	139	−4.02			
			28	−2.80	−2.31
263	167	−1.58			
			72	−1.36	−3.28
335	239	−1.14			

[a]Since the first bottle sample was taken at day 105, a constant respiration rate is assumed for the first 9 days of the upwelling season (row 1).
[b]A constant respiration rate value is used prior to data collection.

estimate the spring transition. Based solely on wind forcing, *Pierce et al*. [2006] select the spring transition date using a statistical change-point detection method to indicate the regime shift from downwelling-favorable winds in wintertime to upwelling-favorable winds in the summertime. For the interannual analysis, low-pass filtered density, dissolved oxygen, and cross-shelf and along-shelf current records from SH70 are shifted to begin on the spring transition date (year: Julian Day, 2009:134, 2010:161, 2011:106) for each respective year. Cumulative wind stress and the spring and fall transition dates are currently available: http://damp.coas.oregonstate.edu/windstress/.

[18] As an alternative to the wind forcing-based spring transition, we define the start of the upwelling season based on in situ measurements. As isopycnals tilt upward and the onshore flow of source water reaches the shelf, values of temperature and salinity on the shelf reflect offshore values. A spring transition date is determined by the intersection of shelf mooring temperature and salinity time series (SH70 supplemented with NH10 in early 2009) with the glider-measured NH25 source water time series annual average (e.g., 2009: 7.4°C, 33.9 psu) within 1 standard deviation (year: Julian Day, 2009: 96, 2010: 167, 2011: 127). This index identifies the arrival of upwelling waters onto the shelf which influence near-bottom biogeochemical processes and early-season ecosystem dynamics.

[19] The rate of oxygen decline during each upwelling season is analyzed by fitting linear regression lines to DO time series. Each DO time series is first shifted by the source water-based spring transition date, described above. The fall transition, or end of upwelling season, date marks the increase from source water to wintertime shelf temperatures. DO values less than the source water average concentration (2.3 mL L^{-1}) of each time series are used in the interannual analysis in order to exclude events with elevated measurements (e.g., day 18 and 60 in 2009) and to capture the lower frequency secular trend due to shelf processes over a season. Minimum DO values corresponding to $\sigma_t = 26.5 \pm 0.1$ kg m^{-3} are used in the least-squares linear regression line calculation. The minimum values are selected using a change-point detection algorithm with a tolerance of 0.2 mL L^{-1}.

3. Results

3.1. Current and Density Structure

[20] Off the central-Oregon coast, upwelling-favorable winds drive an equatorward coastal jet that is deflected around the submarine Heceta and Stonewall Bank complex [*Castelao and Barth*, 2005]. Moored current records from SH15, LB15, SH70, and NH10 (2009) and COAST (2001) locations are analyzed to compare the mean and variability of currents (Figure 3). Depth-average current vectors show the mean equatorward flow at all locations except for SH70, located in the lee of the Bank, confirming previous results [*Barth et al*., 2005]. Currents at the inner shelf site

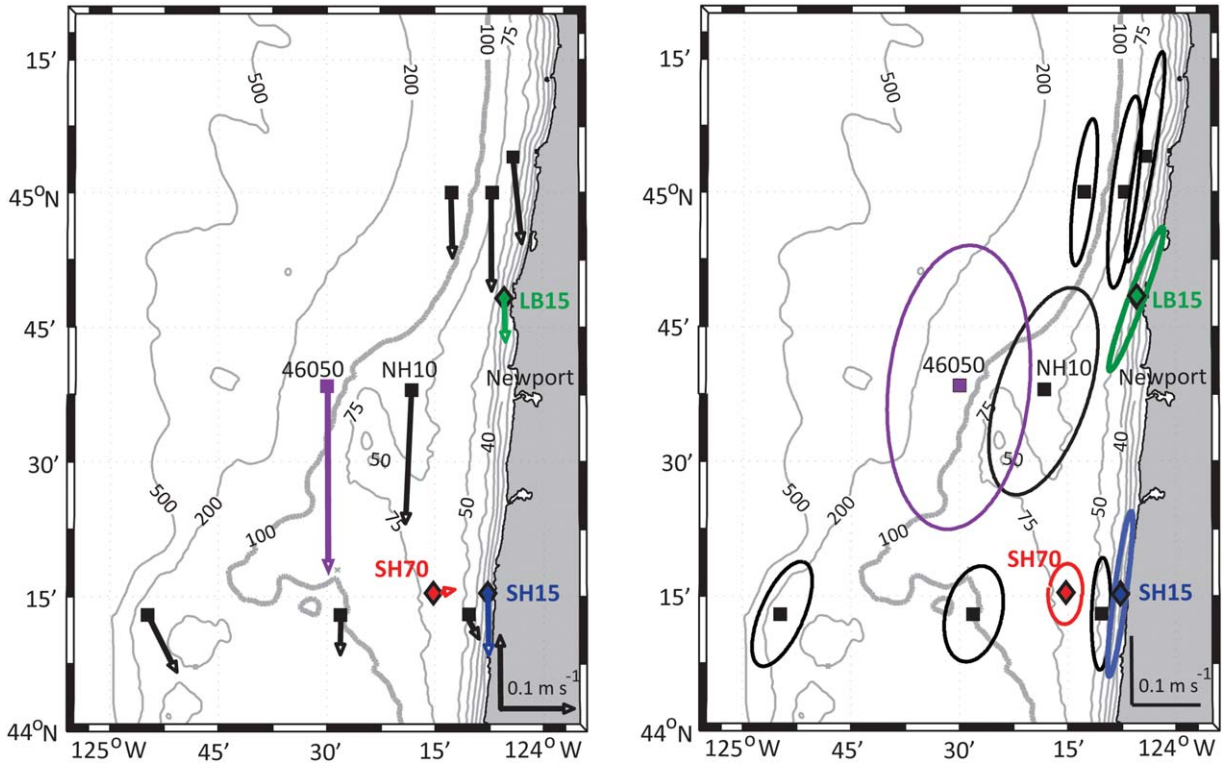

Figure 3. Depth-averaged (left) velocity vectors and (right) variability ellipses for mooring locations described in section 2.1. Wind velocity data from NDBC 46050 are scaled down to 1/10 original magnitude. Semimajor (-minor) axis lengths of ellipses are equivalent to the standard deviation of depth-averaged along-shelf (cross-shelf) velocities at each location: black (COAST 2001 and NH-10 2009); green (Lincoln Beach 15 m water depth 2009—LB15); blue (Strawberry Hill 15 m water depth 2009—SH15); and red (Strawberry Hill 70 m water depth 2009—SH70).

east of the Bank (SH15) agrees strongly with the inner shelf site north of the Bank (LB15) demonstrating the effect on currents from the Bank does not translate to the inner shelf. This also suggests connectivity between inner shelf sites (SH15, LB15). *Kirincich and Barth* [2009] introduce the idea of a second upwelling jet on the inner shelf, inshore of the Bank. Current variability ellipses (Figure 3) show strong north-south variability north of the Bank and an increase in the cross-shelf component of current variability over the Bank except for the inner shelf sites (SH15, COAST SIS). This supports the deflection of the coastal jet moving offshore [*Barth et al*., 2005] as the upwelling season develops. Mean and fluctuation states of the midshelf location, SH70, are anomalously weak and less polarized compared to the inner shelf. Currents at SH15 and LB15 are polarized in the along-shelf direction, in agreement with the 15 m isobath and the mean wind direction.

[21] In the vertical, mean southward and offshore surface flow and onshore return flow in the interior is expected [*Winant et al*., 1987; *Smith et. al*., 1981; *Huyer et al*., 1979]. Mean vertical profiles from the inner shelf (SH15, LB15) show southward along-shelf and near-zero depth-integrated cross-shelf flow (Figure 4). The midshelf is anomalous with a cross-shelf mean directed onshore and weakly northward. Along-shelf vertical shear suggests subsurface, poleward pressure-driven flow opposing the direction of the wind-driven currents. The uniform onshore flow at SH70 indicates a deviation from wind-driven Ekman surface transport over the bank due to flow-topography interaction.

[22] Vertical density profiles show the structure of stratification during upwelling at SH15, LB15, and SH70 (Figure 4c). Qualitatively similar, the inner shelf sites have weaker stratification and a relatively thicker upper mixed layer (~40 versus ~10%) than the midshelf site. This indicates vertical, diapycnal advection and mixing processes are more restricted on the midshelf. During downwelling, a lighter and well-mixed water column is observed on the inner shelf, whereas only the thicknesses of the boundary layers of the midshelf density structure change (not shown). The thickness of the bottom mixed layer at SH70 (~20%, or 14 m) yields an estimate for the vertical extent of near-bottom low-oxygen waters for the midshelf.

3.2. Subtidal Variability

[23] Low-pass filtered (>40 hr, <seasonal) time series of wind stress and moored near-bottom temperature, salinity, dissolved oxygen, and cross- and along-shelf velocities at inner shelf sites SH15 and LB15 and the midshelf site SH70 during the upwelling season of 2009, reveal differences in low-frequency variability across the shelf (Figure 5). With a higher dynamic range than the midshelf, the inner-shelf records cycle from high to low oxygen at a period of ~30 days that is significantly correlated with along-shelf wind stress (Table 3). This cycle can be explained by wind-driven coastal upwelling circulation. During upwelling-favorable wind events, low-oxygen bottom waters are transported to the inner shelf, decreasing the cross-shelf gradient in DO (Figure 5; SH15 and SH70). The opposite is observed during downwelling-favorable wind events, when the cross-shelf difference in DO exceeds 6 mL L^{-1} (SH15 and SH70). A similar cycle is evident in temperature

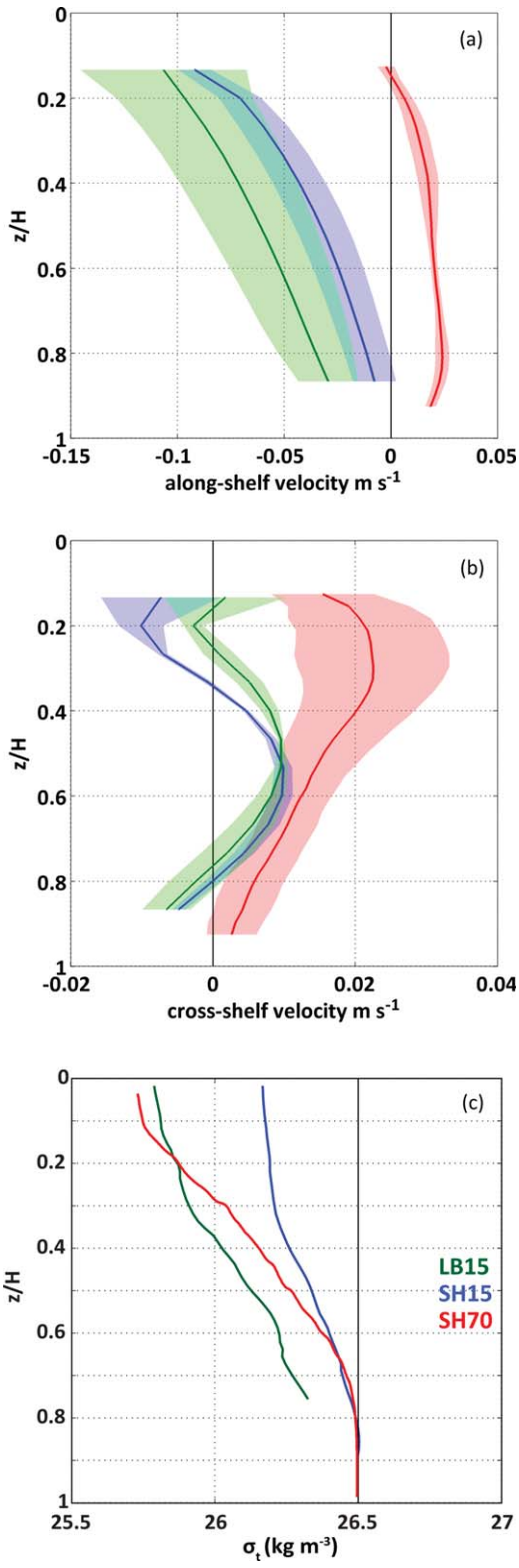

Figure 4. Depth profiles of (a) along-shelf and (b) cross-shelf velocities averaged over three field seasons (2009–2011), with standard deviation shaded, at SH15 (blue), LB15 (green), and SH70 (red). Positive velocities represent northward and onshore flows. (c) Ship-cast density data show typical vertical structure during upwelling. The vertical axis, z/H, is measurement depth normalized by water depth where 0 is the surface and 1 is the bottom.

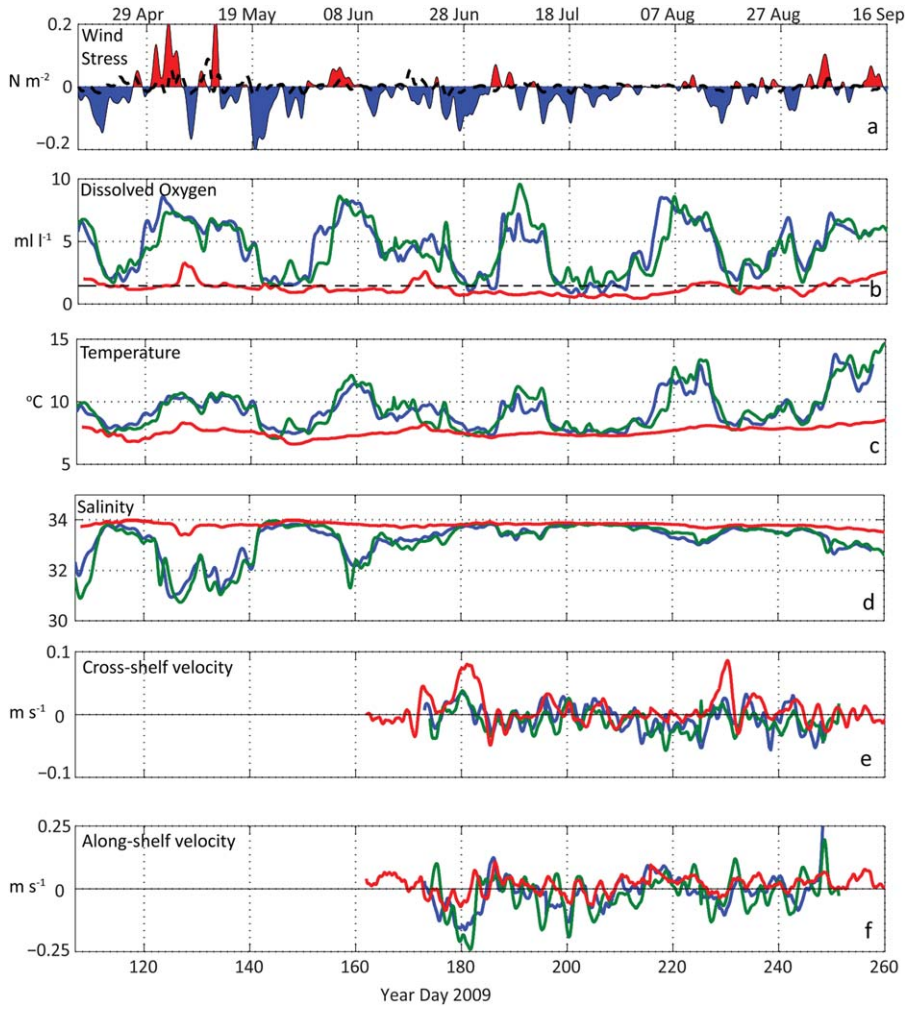

Figure 5. (a) Low-pass filtered time series (2009) of north-south wind stress component from NDBC Buoy 46050 with positive (red) and negative (blue) values corresponding to downwelling-favorable and upwelling-favorable conditions, respectively. (b-f) Low-pass filtered near-bottom dissolved oxygen, temperature, and salinity, cross-shelf velocity and along-shelf velocity observations from inner-shelf (13 m depth in 15 m of water) SH15 (blue) and LB15 (green), and midshelf (68 m depth in 70 m of water) SH70 (red) moorings indicate stronger cross-shelf variability than along-shelf variability for the 150 day overlapping time record. The hypoxic threshold, or dissolved oxygen concentrations below 1.4 mL L^{-1}, is plotted as a dashed line in Figure 5b, the dissolved oxygen plot.

Table 3. Maximum, Time-Lagged, Cross-Correlation Coefficients Calculated Between Along-Shelf Wind Stress and Observed Variables[a]

	SH15	LB15	SH70
Oxygen	0.63 (46)	0.65 (53)	0.24[b] (82)
Temperature	0.53 (53)	0.54 (54)	0.37 (197)
Salinity	−0.56 (54)	−0.53 (57)	−0.37 (216)
$u_{depth\text{-}avg}$	0.42 (225)	−0.28 (312)	−0.57 (27)
$u_{near\text{-}bottom}$	−0.80 (3)	−0.70 (5)	−0.69 (10)
$u_{near\text{-}surface}$	0.56 (−1)	0.52 (−2)	0.37 (3)
$v_{depth\text{-}avg}$	0.75 (7)	0.82 (7)	0.64 (4)
$v_{near\text{-}bottom}$	0.71 (4)	0.82 (7)	0.55 (−2)
$v_{near\text{-}surface}$	0.78 (5)	0.82 (5)	0.54 (10)

[a]Corresponding lags (hours) are in parentheses. Wind leads observed variables for positive lags.
[b]Not within 95% confidence interval.

and salinity (Figure 5), suggesting that low-frequency variability of DO is driven by a physical mechanism: advection via wind-driven upwelling currents. A ∼30 day cycle observed in the inner-shelf indicates intraseasonal oscillations, previously found to be due to fluctuations in the location of the Jet Stream [*Bane et al*., 2007]. Air-sea oxygen fluxes could also cause an increase in near-bottom DO on the inner shelf during times of low stratification; however, the event-scale DO cycles observed in 2009 are strongly related to changes in density most likely due to upwelling and downwelling currents.

[24] Near-bottom current records (Figures 5e–5f), however, have a higher frequency variability, ∼2–5 days, similar to the wind record. On day 180 of 2009, during an upwelling-favorable wind event, southward and onshore near-bottom currents at SH15, LB15, and SH70 were observed. Current response to downwelling-favorable wind events is more

complicated. On day 245, during a downwelling-favorable event, offshore near-bottom currents are observed on the inner shelf and a response in the midshelf record occurs a few days later. Correlation analysis results quantify the relationships between the wind record and moored observations (Table 3). Although wind-current correlations are similar across the shelf, wind-DO correlations are larger on the inner shelf due to the strong, cross-shelf gradients advected on the inner shelf between upwelling and downwelling. Furthermore, a positive correlation of wind and near-bottom alongshelf currents at SH70 indicates the strong effect of an alongshelf pressure gradient when upwelling-favorable winds weaken or reverse [*Barth et al*., 2005].

[25] To quantify the variation of currents across the Bank, cumulative displacements, or time integrated currents, [*Kirincich and Barth*, 2009; *Send and Nam*, 2012] are calculated for the 2009 near-bottom current records. Cumulative displacement (CD) represents the total distance a water parcel travels over time. Along-shelf CDs at the two inner-shelf sites agree well with each other and with the cumulative along-shelf wind stress (Figure 6); however, cross-shelf CDs are weak and slightly offshore. North of the Bank, the along-shelf CD for the NH10 mooring agrees with the wind record, but is larger in magnitude than on the inner-shelf, indicating stronger or more persistent southward currents. Cross-shelf CD at NH10 is offshelf, indicating that the onshore compensatory flow balancing the offshore surface Ekman transport is in the interior. The SH70 site is anomalous with onshore and northward along-shelf CD over the season, indicating a recirculation pathway on shore of the Bank and a more retentive, less wind-driven location.

[26] Cumulative hypoxia, or the total time DO < 1.4 mL L^{-1} is observed throughout a season, is an indicator of the frequency of low-oxygen events for each location. Based on the overlapping data records of 2009 (Figure 5), cumulative hypoxia results are 3 days (4% of record) at LB15, 12 days (12%) at SH15, and 104 days (73%) at SH70, indicating a large cross-shelf gradient in hypoxic measurements from 15 to 70 m water depth (10 km cross-shelf distance) and a slight along-shelf gradient between the two inner shelf moorings (60 km along-shelf distance). The midshelf site (SH70) located over Stonewall Bank measures hypoxic water for the majority of the observed season.

3.3. High-Frequency Variability

[27] High-pass filtered (<40 h) DO records from the three moorings SH15, LB15, and SH70 show a high-frequency range of ± 2 mL L^{-1} on the inner shelf (Figure 7b). The high-frequency variability of DO on the midshelf is low (< 0.5 mL L^{-1}) yielding two possible scenarios: high-frequency currents differ greatly from the inner shelf or the gradient of midshelf DO is low over the length scales affected by the high-frequency currents.

[28] High-pass filtered, depth-averaged currents at SH15, LB15, and SH70 (Figures 7d and 7e) were analyzed using T_Tide [*Pawlowicz et al*., 2002], a harmonic regression analysis tool. The diurnal (K1) and semidiurnal (M2) amplitudes (m s^{-1}) for along and cross-shelf current variability are shown in Table 4. At the northern site (LB15), a mixed, semidiurnal tide with M2 along-shelf amplitude greater than K1 is found. Since the barotropic tidal velocities are similar

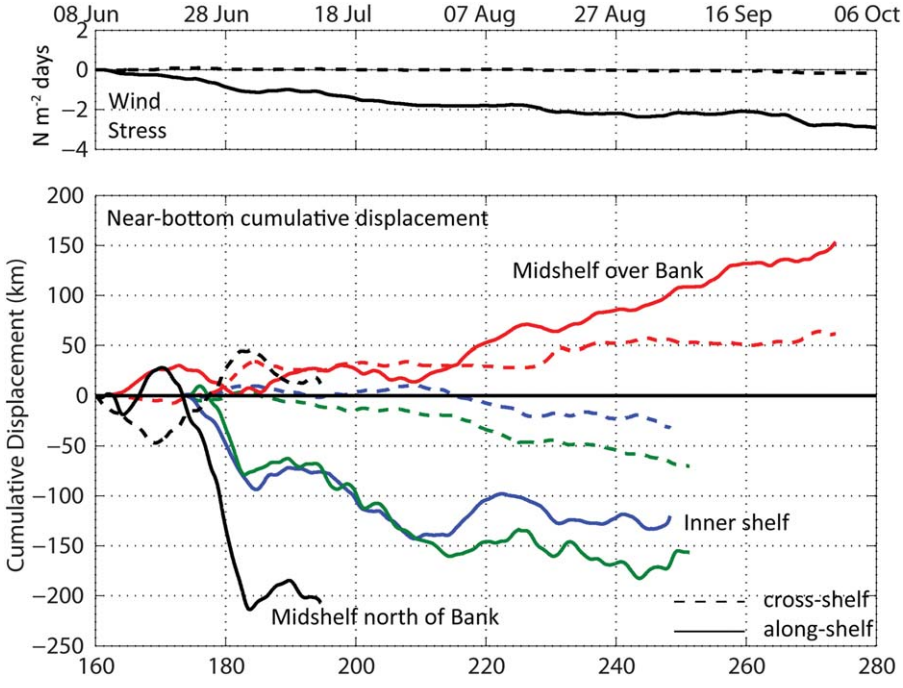

Figure 6. Cross-shelf (dashed) and along-shelf (solid) wind stress (NDBC 46050) and cumulative displacements at inner-shelf [SH15 (blue) and LB15 (green)] and midshelf [SH70 (red) NH10 (black)] mooring locations based on low-pass filtered, near-bottom current velocities. Near-bottom sampling depths are 65 m for SH70, 75 m for NH10, and 12 m for inner shelf moorings. Positive values represent northward and onshore flows.

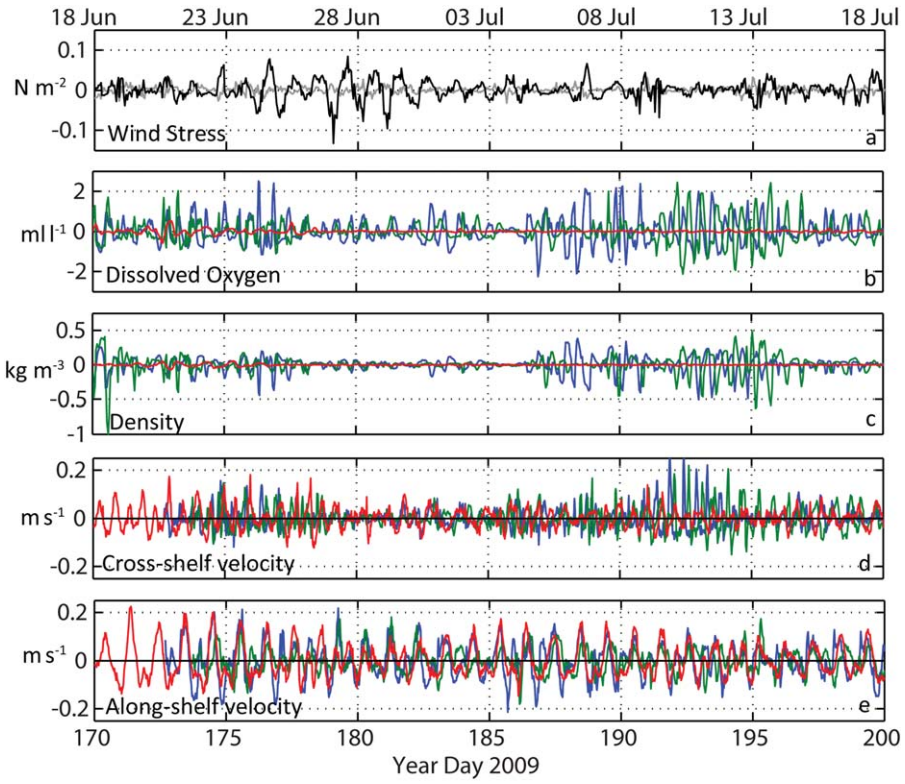

Figure 7. High-pass filtered (a) along-shelf (black) and cross-shelf (gray) wind stress (NDBC 46050), (b) DO, (c) temperature, (d) salinity, and (e) cross-shelf and (f) along-shelf depth-averaged velocity time series from LB15 (green), SH15 (blue), and SH70 (red) mooring locations from 2009.

between the inner (SH15) and midshelf (SH70) along 44.25°N, we conclude that the presence of tidal-band variations in dissolved oxygen on the inner shelf are a result of advection of horizontal gradients—higher oxygen present shoreward of the 15 m inner shelf mooring—and their absence at the midshelf is because horizontal gradients of dissolved oxygen are low there.

[29] Note that the diurnal (K1) tidal constituent is dominant at SH15 and SH70, indicating agreement in tidal velocity variability across the shelf along 44.25°N and a variation in the along-shelf direction. The along-shelf current variability amplitudes explained by the K1 and M2 constituents are four times greater at SH15 and SH70 than at LB15. This result is supported by previous modeling work [*Erofeeva et al*., 2003; *Osborne et al*., 2011] and verification of model results with COAST mooring data (Figure 1) (J. Osborne, personal communication, 2013) which show a resonance of coastal shelf waves at tidal frequencies (K1, M2) due to the geometry of the Bank.

[30] Mechanisms other than advection of horizontal oxygen gradients by the barotropic tide may contribute to the high-frequency variability of oxygen on the inner shelf (± 2 mL l^{-1}). Off Southern California, nonlinear internal waves observed on the inner shelf result in cold water intrusions and enhanced near-bottom mixing [*Nam and Send*, 2011], both of which may impact near-bottom oxygen variability. Nonlinear internal tides are frequently observed in the SH15 and LB15 temperature and velocity records [*Suanda and Barth*, 2012].

Table 4. Tidal Current Amplitudes and Tidal Excursion Estimates Due to K1 and M2 Tidal Constituents Based on Depth-Averaged 2009 Data Records

	K1 Amplitude ($m\ s^{-1}$)	K1 Tidal Excursion (km)	M2 Amplitude ($m\ s^{-1}$)	M2 Tidal Excursion (km)
Along-Shelf				
LB15	0.02	0.55	0.03	0.43
SH15	0.07	1.9	0.06	0.85
SH70	0.08	2.2	0.05	0.71
Cross-Shelf				
LB15	2.6×10^{-3}	0.07	6.8×10^{-3}	0.10
SH15	1.3×10^{-3}	0.04	8.4×10^{-3}	0.12
SH70	0.01	0.27	0.02	0.28

[31] Tidal excursion estimates for the K1 and M2 are calculated by integrating over half of a tidal cycle

$$TE = A_{K1} \int_{0}^{0.5 \cdot T_{K1}} \sin\left(\frac{2\pi}{T_{K1}} t\right) \mathrm{d}t$$

where A_{K1} is the amplitude of current variability (m s^{-1}) and T_{K1} is the K1 tidal period (23.93 h). Along-shelf and cross-shelf tidal excursion estimates for the K1 and M2 (Table 4) give a spatial bound of the region over the Bank vulnerable to hypoxia: 4.4 km (1.42 km) in the along-shelf (cross-shelf).

3.4. Interannual Variability

3.4.1. Density and Oxygen

[32] Time series of near-bottom density anomaly (σ_t) and dissolved oxygen (DO) observations from three upwelling seasons (2009–2011) from the midshelf mooring site (SH70; 70 m water depth) are presented in Figure 8a. A clear spring transition from wintertime (relatively warm, fresh, and high-oxygen water) to summertime values on the midshelf is evident in early April 2009 (day 96), mid-June 2010 (day 167), and early May 2011 (day 128) (Figure 8a). The fall transition is most evident in mid-September 2011 (day 236) with a sharp transition due to a storm event, characterized by positive wind stress (not shown) when oxygen increased 1 mL L^{-1} day^{-1} for 4 days.

[33] As each upwelling season progresses, density values approach ~26.5 kg m^{-3}. Dissolved oxygen time series, however, decline at a near-linear rate, quantified and discussed further below. Hypoxia (DO < 1.4 mL L^{-1}) is observed at this location for 104 d (2009), 81 d (2010), and 110 d (2011).

[34] Realigning the midshelf DO time series of each year to start on the respective spring transition date allows for a comparison based on the start of the upwelling season rather than calendar date (Figures 8a–8c). The time evolution of the shifted time series has a few key differences. First, the values of density and dissolved oxygen at the beginning of upwelling (day 0) are different between the years. Second, the 2009 DO time series now begins at a near-hypoxic value and hypoxic measurements were made days 12–18 before the start date to the upwelling season (day 134) indicating that the transition to summertime conditions (colder, saltier, lower in oxygen) occurred prior to day 134. Third, shifted density measurements reach a "steady state" σ_t value (26.5 kg m^{-3}) between days 60 and 80 of each upwelling season. During this time period, while waters of nearly equal density are measured each year, DO content in 2009 is on the order of 0.5 mL L^{-1} lower than in 2010 and 2011 (Figure 8b).

[35] As established above, the spring transition dates as determined by wind alone [*Pierce et al.*, 2006] do not fully capture the low-oxygen season observed on the shelf each year (Figures 8a and 8b). A disconnect between spring transition dates based on wind forcing and in situ measurements has been previously observed [*Kosro et al.*, 2006]. Hence, we define an alternative spring transition date, based on in situ data (see section 2.2). Shifting density and dissolved oxygen time series by these new dates (Figure 8c) reveal remarkable similarity between years, with the

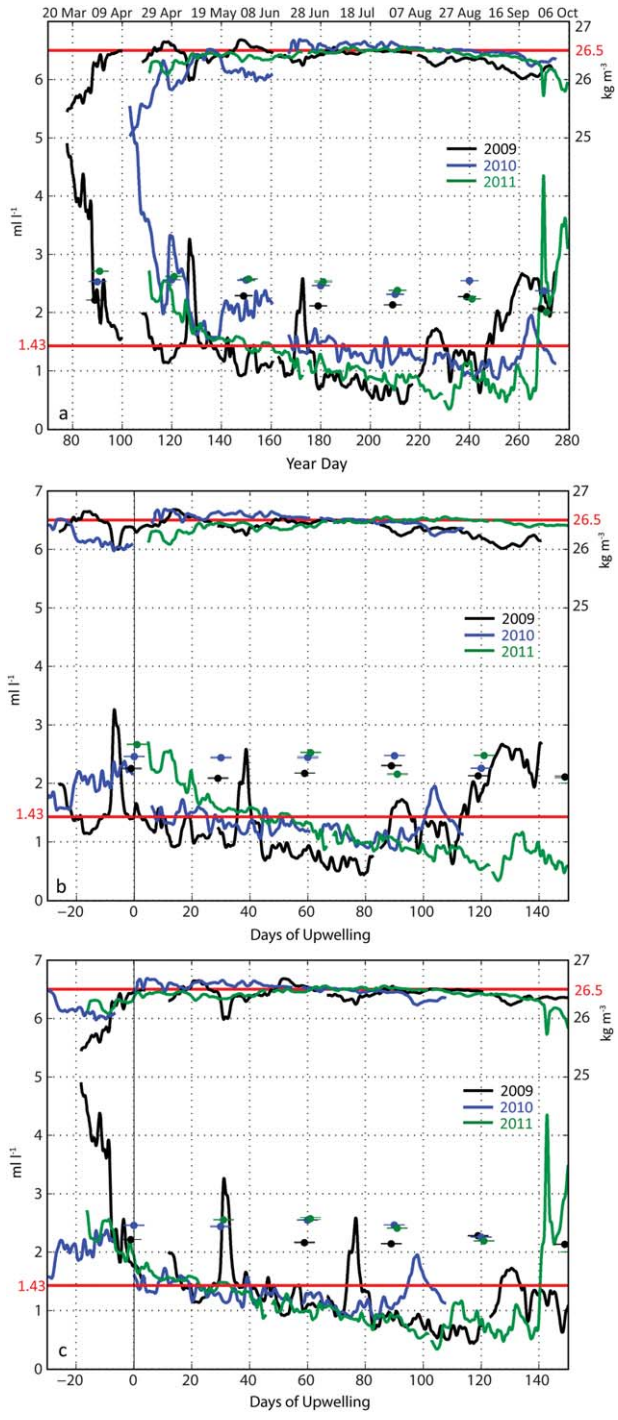

Figure 8. (a) Dissolved oxygen and σ_t (density—1000 kg m^{-3}) time series at SH70 for the 2009 (black), 2010 (blue), and 2011 (green) upwelling seasons with the 30 day average glider data from NH25 (σ_t 26.5 kg m^{-3}) (filled circles). (b) Shifting by the respective start day of upwelling (2009:134, 2010:161, 2011:106) based on wind forcing shows water with equal density (26.5 kg m^{-3}) and differing oxygen concentrations around 75 days into the upwelling season. (c) Shifting by the spring transition date based on source water data (2009: 96, 2010: 167, 2011: 127) shows strong agreement throughout each respective season.

exceptions of the two distinct high-oxygen events in 2009 near days 30 and 75. With this new shifting, values of dissolved oxygen and density are similar at the beginning of each upwelling season (day 0), the time series agree throughout most of the upwelling season and a near-linear decline in oxygen is evident. Furthermore, with the new shifting, the variability between years is controlled principally by the slope of the decline and the length of each season (Figure 8c). Each upwelling season begins with approximately equal DO concentrations, which are lower than glider-measured source water DO concentrations. The absolute minimum oxygen value observed each year occurs within a week or two of the fall transition. The time separating the spring and fall transition dates yields upwelling season lengths of 121, 92, and 109 days for 2009–2011.

3.4.2. Currents

[36] Mean depth profiles of SH70 current records are very similar between years (Figure 4), indicating no significant change of currents averaged over each upwelling season. Time series of cumulative displacements (CD) are calculated, following *Kirincich and Barth* [2009], for the midshelf (SH70), near-bottom (~65 m) cross-shelf and along-shelf components of velocity (Figure 9b). The CDs on the midshelf over the Bank are poleward and onshore. Poleward displacement at the SH70 location is opposing the direction of the local wind forcing and further supports the influence of a poleward along-shelf pressure gradient [*Barth et al*., 2005]. Changes in cross-shelf displacement on the order of the midshelf width (30 km at SH70) occur over 10–30 day periods (Figure 9b). These estimated residence times suggest it can take up to 1 month for water to move on or off the shelf at this location. The stretches of time when cross-shelf CD does not change are periods when flushing rates are lowest on the shelf and biological processes are expected to have an increased effect on oxygen decline.

[37] In 2010, a persistent (~20 day) positive (onshore) near-bottom flow is observed (days 190–210, Figure 9b) during a strong upwelling-favorable period in the wind record (Figure 9a). The strong, uninterrupted near-bottom return flow during 2010 is expected to have a flushing effect on shelf waters to replenish near-bottom oxygen levels to source water concentrations as discussed in section 3.4.5.

3.4.3. Winds

[38] Analysis of offshore wind stress for each upwelling season (as defined in section 2.2 based on in situ source water temperature) indicates interannual variability in the cumulative along-shelf wind stress and the occurrence of wind reversals. Cumulative along-shelf wind stress, used as a proxy for upwelling intensity, varies between years (year-day: stress in N m^{-2} day^{-1}: 2009: −2.57; 2010: −3.26; 2011: −1.57; Table 5; Figure 9a). This metric shows that stronger upwelling-favorable winds occurred in 2010 than in other years. Stronger winds suggest stronger advective currents, as evident in Figure 9c. The ratio of upwelling-favorable wind events to downwelling-favorable wind events, defined by the cumulative time negative:positive along-shelf wind stress was measured, also differs significantly (Table 5). Downwelling relative to upwelling was

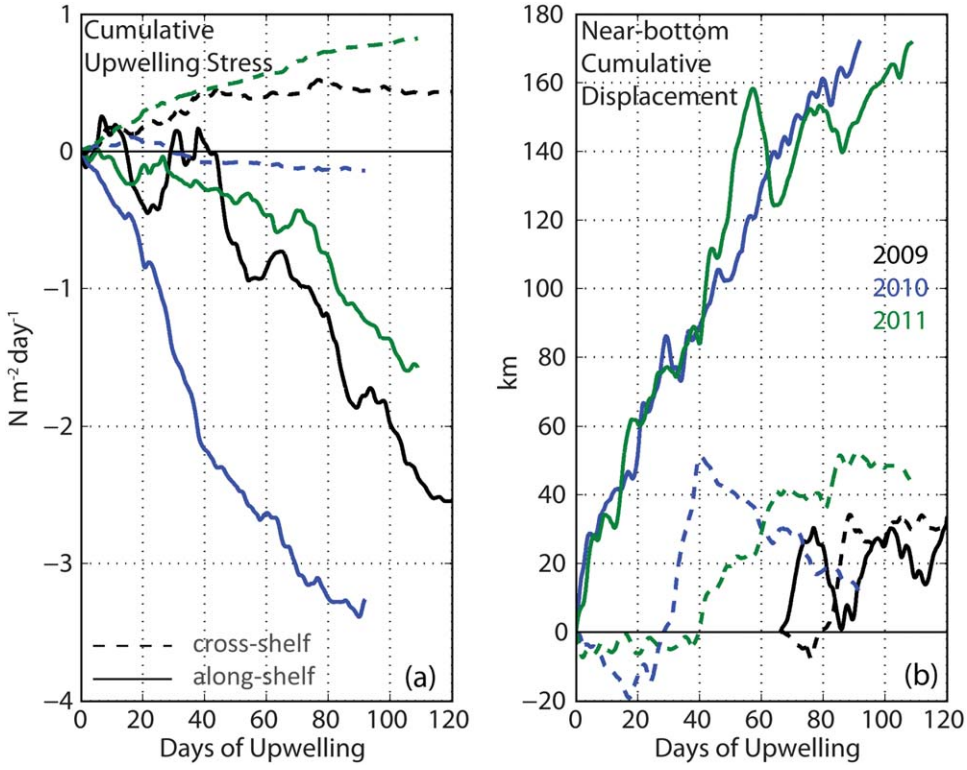

Figure 9. Interannual comparison of (a) cumulative wind stress (NDBC 46050) and (b) near-bottom (~65 m) cumulative displacements (SH70) for the 2009 (black), 2010 (blue), and 2011 (green) upwelling seasons. Positive values indicate northward or eastward (onshore) directions.

Table 5. Interannual Wind Statistics for NDBC 46050 North-South (Along-Shelf) Wind Stress, Derived Using *Large et al*. [1994] Drag Coefficients During the Upwelling Season, as Defined in Section 2.2[a]

	Length of Season (days)	Cumulative Wind Stress (N m^{-2} day)	% Upwelling Favorable Events	Upwelling: Downwelling Favorable Events
2009	121	−2.57	67.9	2.1
2010	92	−3.26	84.3	5.4
2011	109	−1.57	70.1	2.3

[a]Upwelling-favorable wind events are defined by negative wind stress.

higher in 2009 and 2011 than in 2010. Furthermore, in 2009 (2010) (2011), upwelling favorable winds were observed 2.1 (5.4) (2.3) times more than downwelling favorable winds. This ratio is indicative of the distribution of upwelling over a season rather than the total amount which may be of first-order importance to biological communities and biogeochemical cycles on the shelf (A. Galan, personal communication, 2012).

3.4.4. Source Water

[39] Coastal upwelling brings cold, salty, oxygen-poor, and nutrient-rich water, here called source water, onto the central-Oregon shelf each year. Source water dissolved oxygen concentrations are low, but are above the hypoxic threshold of 1.4 mL L^{-1}. While the exact source water pathway over the Bank is not known, earlier work suggests that source water may originate from the slope southwest of the Bank [*Castelao and Barth*, 2005]. In the absence of data from this part of the slope, glider data (30 day averages, σ_t of 26.5 ± 0.01 kg m^{-3}) of waters from NH25 (Figure 1), along the Newport-hydrograph line are used as a proxy for source water over the Bank due to its location over the slope. DO values at σ_t of 26.5 kg m^{-3} are higher (>2 mL L^{-1}) at NH25 than measurements on the shelf (<1.4 mL L^{-1}; Figure 8). A strong correlation between glider-measured source water DO and density is calculated for 2009–2011 (Figure 10). For a 0.1 kg m^{-3} change in density, a ∼0.32 mL L^{-1} change in oxygen is observed at NH25. The interannual variability of average source water DO concentration at σ_t of 26.5 kg m^{-3} is *O* (0.1 mL L^{-1}). Source water concentrations are above the hypoxic threshold indicating hypoxic waters are not advecting onto the shelf from offshore.

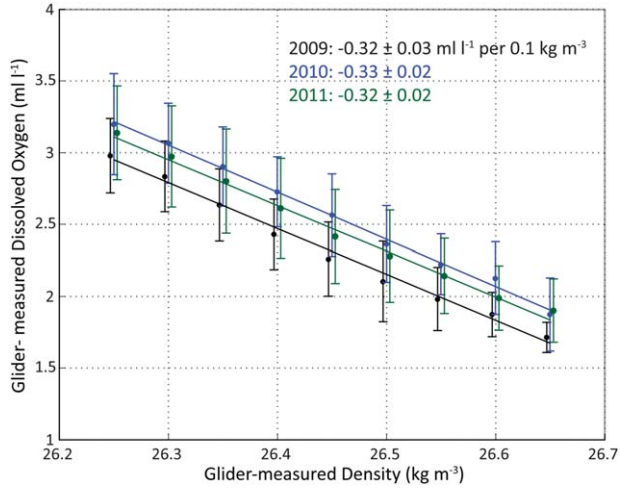

Figure 10. Source water DO-density relationship from glider-measured data at NH25 for 2009–2011 averaged over each respective upwelling season, indicating ∼0.32 mL L^{-1} change in DO per 0.1 kg m^{-3}.

[40] Differences between 30 day averaged source water (glider; NH25) and shelf (SH70) dissolved oxygen measurements reveal a seasonal cycle (Figure 11). During wintertime, the shelf is ventilated due to strong mixing and advection yielding higher DO concentration over the slope. During the upwelling season, the DO levels on the shelf decrease 1.5 mL L^{-1} below source water concentrations, due to shelf processes such as microbial respiration. Interannual variability in the phase and amplitude of this cycle is observed. If source water concentrations controlled DO levels on the shelf, this annual cycle would level off near zero after the spring transition assuming the DO concentration of source water is constant. The fall transition marks the end of the upwelling season as shelf DO increases due to the increased mixing associated with strong winter storms.

3.4.5. Net Dissolved Oxygen Decline

[41] At the beginning of the upwelling season, dissolved oxygen concentrations on the shelf sharply decrease to

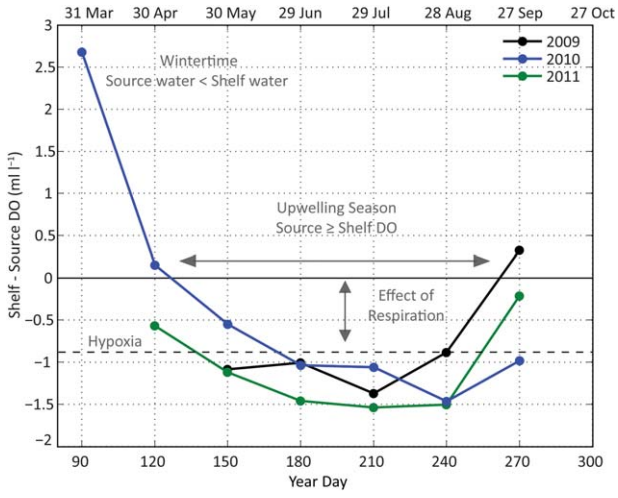

Figure 11. Difference between 30 day average of dissolved oxygen measurements from NH25 (glider, 26.5 ± 0.01 σ_t) and SH70 (near-bottom) for the 3 years of the study. A positive (negative) value indicates higher dissolved oxygen over the shelf (shelf break). Hypoxia is indicated by the dashed line with a value of 0.87 mL L^{-1}, the difference between average source water DO concentration (∼2.3 mL L^{-1} for 26.5 kg m^{-3} σ_t) and the hypoxic threshold (1.4 mL L^{-1}).

source water levels (>2 mL L^{-1}) and continue to decline due to biogeochemical consumption. A low-frequency, near-linear decline is apparent in the shifted SH70 DO time series (Figure 8c). This observed decline during the upwelling season is modulated by respiration, advection, and mixing. To determine and quantify which processes control the rate of oxygen decline on the shelf, linear regression lines are fitted to DO and density time series at LB15, SH15, and SH70 (2009–2011). Midshelf SH70 net DO decline rates of $-1.0 \pm 0.1 \times 10^{-2}$ ($-0.5 \pm 0.2 \times 10^{-2}$) ($-1.0 \pm 0.2 \times 10^{-2}$) mL L^{-1} day^{-1} result in a decrease of ~0.3 mL L^{-1} per 30 days (Figure 12a). The lower rate of decline in 2010 agrees well with the onshore near-bottom transport of source water and prolonged upwelling-favorable winds (Figure 9a) (sections 3.4.1 and 3.4.2). The inner-shelf sites (LB15 and SH15) experience high-oxygen events the majority of the upwelling season. A linear decline of low-oxygen events is observed at SH15 but not at LB15 (not shown). The net observed decline of DO along 44.25°N (SH15 and SH70) suggests a pathway of onshore flow from SH70 (cumulative hypoxia ~90 days) to SH15 (cumulative hypoxia ~12 days) and is important for nearshore biological communities, especially during years of severe hypoxia [*Chan et al*., 2008].

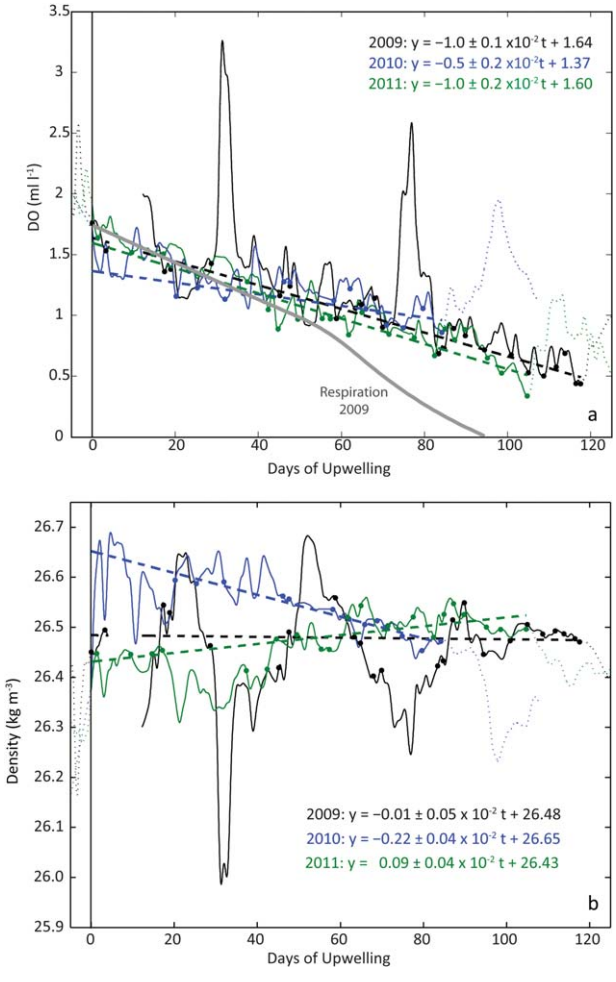

Figure 12. (a) Near-bottom oxygen and (b) density measurements at SH70, shifted by start of upwelling season date based on in situ source water data (described in section 2.2). Linear regression lines (dashed) are fitted to minimum oxygen measurements less than source water concentrations (2.2 mL L^{-1}) corresponding to density 26.5 ± 0.1 kg m^{-3} (filled circles). Net oxygen decline rates, or regression line slopes, are less than the decline expected from near-bottom bottle respiration rates (gray) from 2009 (Table 2). Regression line slopes and offsets are above 95% significance level.

[42] Comparing the midshelf net DO decline rates to the pelagic respiration rates measured at SH70 during 2009 (Table 2), we find that the observed seasonal rates of decline are less than that expected due to respiration alone. Interpolating respiration rates between samples yields a biologically induced DO decrease of ~3 mL L^{-1} over an upwelling season. An oxygen sink of this magnitude would result in anoxia approximately 95 days into the 2009 upwelling season (Figure 12a); however, anoxia was not observed. This result indicates that the rate of DO decline on the shelf is restricted due to the physical (advection, mixing) processes, not the availability of organic matter. Rates of change on shorter time scales (2–5 days) are much higher than respiration rates (Figure 12a). These sharp changes in oxygen concentration can be explained by advection of gradients, not local biogeochemical properties.

[43] As presented in Figure 10, an oxygen decline of 0.32 mL L^{-1} is expected for a 0.1 kg m^{-3} decrease in source water density. The contribution of density changes to the observed oxygen decline at SH70 (Figure 12a), is calculated by fitting linear regression lines to the density time series (Figure 12b) at measurements used in the DO regression analysis. There is no significant change in density over the 2009 upwelling season and a decrease of 0.2 kg m^{-3} in 2010 and an increase of 0.1 kg m^{-3} in 2011 (Figure 12b). Applying the source water DO-density relationship (Figure 10), no significant change in oxygen is expected in 2009 and a change of 0.65 (−0.31) mL L^{-1} is expected in 2010 (2011). The DO variability associated with density changes is due to advection and mixing processes acting across isopycnals.

[44] The relationship of physical:biological mechanisms driving oxygen decline varies between years. To quantify the contribution of the drivers of DO variability at SH70 each year, the effect of respiration (assuming the average rate from 2009 of -2.6×10^{-2} mL L^{-1} day^{-1} × days of upwelling) and density (slopes from Figure 12b × days of upwelling) are subtracted from the observed net oxygen decline rates (slopes from Figure 12a times days of upwelling) revealing a residual which we attribute to advection and mixing processes along the 26.5 kg m^{-3} isopycnal (Figure 13). Positive residuals signify that physical processes (advection and mixing) are responsible for oxygen concentrations on the shelf from reaching the anoxic levels that are anticipated from respiration rates alone. The relative contribution from physical (density + residual) versus biological mechanisms is calculated as (density + residual)/respiration. The 3 year average is (1.7 + 0.1)/2.8, or 64%, contribution by physical processes. Alternatively, the net observed decrease is 36% of the potential draw down expected from microbial respiration. Variations in source water DO concentrations (not presented here) are small in comparison to the net observed rates of the decline (Figure

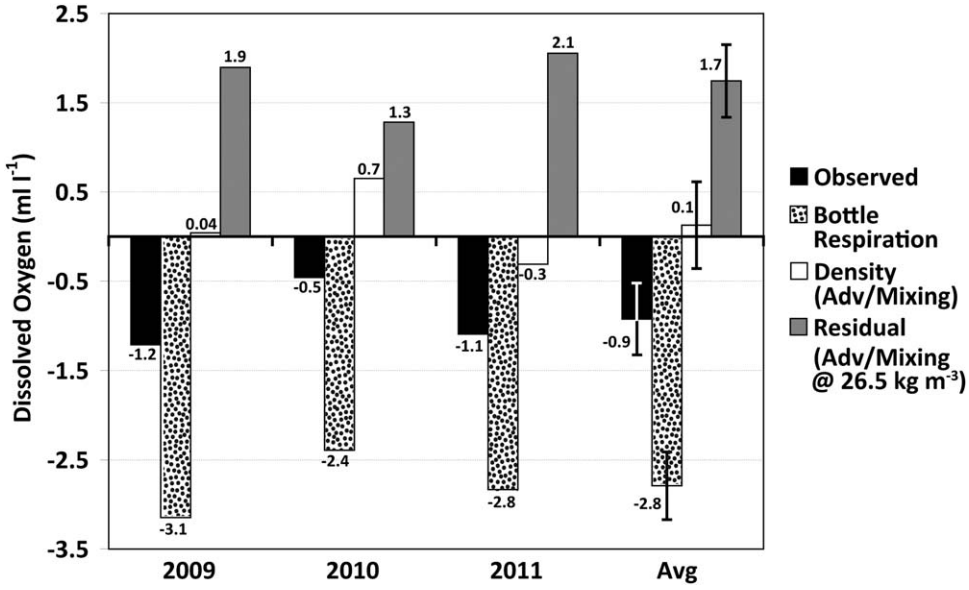

Figure 13. Contributions to oxygen decline (mL L^{-1}) on the midshelf (SH70) from physical and biological processes over each upwelling season, as defined in section 2.2. The observed decrease is calculated from slopes of linear regression lines in Figure 14. Respiration rates are calculated using the average from Table 2: -2.6×10^{-2} mL L^{-1} day^{-1}. Contribution from the change of density is derived from the slopes of linear regression lines of density at SH70 (Figure 12b) and the density-dissolved oxygen relationship calculated for source water (Figure 10). The advection/mixing term is the residual.

12a) and the calculated change in DO due to density (Figure 12b). In 2010, hypoxia was less severe than in other years. We attribute this to the shorter season length (Figure 8, Table 5) and to the decrease in source water density throughout the season (Figures 12b and 13).

4. Discussion and Summary

[45] Dissolved oxygen measurements of near-bottom central-Oregon shelf waters are compared across time bands and across the shelf to investigate driving mechanisms of variability. The analysis of continuous time series of DO reveals event-scale, high frequency (tidal) and seasonal variability not previously resolved with conventional ship-based sampling conducted on the Oregon shelf. The inner shelf (15 m) is well ventilated during reversals or downwelling-favorable wind events and has a low incident rate of low-oxygen, or hypoxic (DO < 1.4 mL L^{-1}), events. The midshelf location (70 m) in the lee of the Heceta and Stonewall Bank complex, however, is less correlated with wind forcing and experiences 98 ± 15 days of hypoxia annually. The Bank is especially vulnerable to low-oxygen events due to the large shelf width, as well as weak currents and high productivity [*Barth et al*., 2005]. Previous ship-based measurements from the 2002 upwelling season indicate hypoxia on the central-Oregon shelf ($\sim$50 m water depths) from July to September ($\sim$90 days) [*Grantham et al*., 2004]. Our results corroborate their finding and paint a clearer picture for ecological implications; hypoxia on the midshelf over the Bank is recurring annually and is present for the majority of each upwelling season.

[46] High-frequency, or tidal band, analysis shows an amplification of K1 tidal currents at the inner and midshelf locations along 44.25°N due to the bank geometry. Near-bottom DO tidal fluctuations are O(2 mL L^{-1}) on the inner shelf and are much less on the midshelf. Variability of this magnitude is an important consideration for ship-based observational studies with duration longer than half an M2 tidal period. Tidal excursion calculations (Table 4) yield spatial estimates for the midshelf low-oxygen zone of 2.2 and 0.27 km in the along and cross-shelf directions, respectively. The M2 internal tide may also contribute to inner-shelf, near-bottom DO fluctuations but is not explicitly studied here.

[47] On seasonal timescales, variability of DO over the Oregon shelf is controlled by physical and biological processes in concert. Wind-driven coastal upwelling initiates low-oxygen events on the shelf via the transport of source water which, off Oregon, has DO concentrations above the hypoxic threshold (1.4 mL L^{-1}). Biological and biogeochemical processes take effect in the productive spring and summer, and the balance of respiration and advection/mixing along with the season length determine the duration of low-oxygen events on the shelf each year. Seasonal decreases in shelf oxygen below source water concentrations range from 0.4 to 1.2 mL L^{-1}, similar to findings on the Washington shelf (0.5–2.5 mL L^{-1}) [*Connolly et al*., 2010]. DO decline rates are linear for the 2009–2011 upwelling seasons. One of the determining factors of how low near-bottom DO concentrations drop, therefore, is the season length. This fits with the 2006 upwelling season, almost 200 days in duration, when anoxia was first observed on the Oregon inner shelf. The average net observed DO decline rate for 2009–2011 (-0.9×10^{-2} mL L^{-1} day^{-1}) is only 32% of the expected decline due to the average water column respiration rate from 2009 (-2.6×10^{-2} mL L^{-1} day^{-1}). This indicates physical processes such as advection and mixing are "flushing" or entraining higher DO water into

the near-bottom environment. In fact, stronger onshore flow supports the less severe hypoxia observed in 2010. Without the contribution from physical processes, anoxia is expected about 90 days into the upwelling season (Figure 12).

[48] Since upwelling source water DO concentrations are above the hypoxic threshold, hypoxia cannot occur on the Oregon shelf without the presence of biological processes (e.g., microbial respiration) (Figure 11); nor on the Washington shelf [*Connolly et al*., 2010]. In addition to the water-column respiration rates presented here, benthic oxygen fluxes into the sediment also contribute to near-bottom hypoxia. *Reimers et al*. [2012], based on a single realization, find Oregon midshelf benthic oxygen consumption ($\sim$1 μM d^{-1} or 2.3×10^{-2} mL L^{-1} d^{-1}) in the sediment surface to contribute to hypoxia. This benthic respiration rate is nearly equal to the pelagic average from 2009 (2.6×10^{-2} mL L^{-1} d^{-1}). Similarly, on the Washington shelf, *Connolly et al*. [2010] found water column respiration rates within the range reported here. Accounting for benthic oxygen flux, the average observed DO decline of 0.9 mL L^{-1} (Figure 13) would change from 32% (pelagic only) to 16% of the expected DO decline due to pelagic and benthic respiration.

[49] By understanding how physical and biological processes affect DO on the shelf, we can project how predicted climate change effects will alter shelf DO concentrations. Based on our analysis, conditions conducive to more severe shelf hypoxia include longer upwelling seasons, denser source water, lower DO source water concentrations, and lower advection and mixing rates. If the effectiveness of physical processes, presently keeping biological processes in check, is diminished, then severe hypoxia or anoxia is expected on the Oregon shelf. Although changes in advection and mixing rates due to climate change are uncertain, source water DO concentrations may decline [*Keeling et al*., 2010].

[50] The source water DO concentration difference between years of O(0.1 mL L^{-1}) does not account for the $\sim$1 mL L^{-1} difference in observed oxygen decline over the 2010 season (Figure 13) or the slower seasonal rate of decline (Figure 12a) compared to other years. Monthly source water averages of temperature, salinity, and oxygen are similar between years unlike the southern California shelf where interannual DO variability, $O(\sim 2$ mL $L^{-1})$ is attributed to El Niño/Southern Oscillation (ENSO) [*Nam et al*., 2011]. Large-scale circulation differences between Oregon and California explain this difference. First, the California shelf is impacted greater by events originating at the equator. Only 40% of the Pacific Equatorial water signal makes it up to Oregon via the CU [*Thomson and Krassovski*, 2010]. Second, the northern part of the CCS is greatly influenced by subarctic water masses [*Whitney et al*., 2007] which may dampen the ENSO signal off the Oregon shelf. Although interannual variability of source water characteristics is small during the 3 years of this study, long-term variability and driving mechanisms of the source water composition upwelling on the Oregon shelf are largely unknown. Understanding source water origins is a future research direction that has important implications for shelf processes during the upwelling season.

[51] The near-bottom time series presented here do not address questions about the vertical structure of hypoxia. Data from the proposed instruments on the National Science Foundation's Ocean Observatories Initiative Endurance array, off Oregon and Washington, will be able to address vertical gradients in physical water properties and oxygen. Vertical resolution is key to understanding the stress exposure to biological communities in the water column as well as to parameterize vertical mixing rates. Biophysical models could be used to address questions left unanswered here regarding the relative importance of benthic versus pelagic respiration or cross-shelf versus along-shelf advective fluxes on near-bottom oxygen dynamics.

[52] **Acknowledgments.** The authors would like to acknowledge the Gordon and Betty Moore Foundation for the support of the MI_LOCO program (grant 1661). This is contribution 440 from PISCO, the Partnership for Interdisciplinary Studies of Coastal Oceans funded primarily by the David and Lucile Packard Foundation and the Gordon and Betty Moore Foundation. We thank our OSU glider group colleagues, specifically K. Shearman, A. Erofeev, Z. Kurokawa, and P. Mazzini, for glider data collection along the Newport Hydrographic line supported by National Science Foundation (NSF) grants OCE-0527168 and OCE-0961999. M. Levine provided the COAST and NH10 mooring data. The NH10 program is funded by the National Science Foundation through the cooperative agreement OCE-0424602 known as CMOP (Coastal Margin Observation & Prediction) and by NOAA through NANOOS (Northwest Association of Networked Ocean Observing Systems), the Pacific Northwest Regional Association of the U.S. Integrated Ocean Observing System (IOOS). Instruments were borrowed from E. Dever, C. Wingard and R. Letelier for the SH70 mooring. We thank SungHyun Nam for his thoughtful review. Special thanks to W. Waldorf, C. Risien, D. Langner, and A. Suanda for invaluable guidance with programming instruments, processing data, and assistance in the field. We thank the marine technicians who assisted with PISCO and MI_LOCO mooring operations: J. Brodersen, K. Page-Albins, B. Focht, T. Rohrer, D. Swensen, D. O'Gorman, and E. Arnesen as well as Captain Mike Kriz and the crew of the R/V Elakha for their data collection efforts.

References

Bane, J. M., Y. H. Spitz, R. M. Letelier, and W. T. Peterson (2007), Intraseasonal oscillations in Oregon's coastal upwelling system: From the jet stream to zooplankton, *Proc. Natl. Acad. Sci. U. S. A.*, *104*, 13,262–13,267.

Barth, J. A., S. D. Pierce, and R. M. Castelao (2005), Time dependent, wind-driven flow over a shallow mid shelf submarine bank, *J. Geophys. Res.*, *110*, C10S05, doi:10.1029/2004JC002761.

Bograd, S. J., C. G. Castro, E. Di Lorenzo, D. M. Palacios, H. Bailey, W. Gilly, and F. P. Chavez (2008), Oxygen declines and the shoaling of the hypoxic boundary in the California current, *Geophys. Res. Lett.*, *35*, L12607, doi:10.1029/2008GL034185.

Boyd, T., M. D. Levine, P. M. Kosro, S. R. Gard, and W. Waldorf (2002), Observations from moorings on the Oregon continental shelf (May–August 2001), Ref. 2002-6, *Data Rep. 190*, Oregon State Univ., Corvallis, Ore.

Castelao, R. M., and J. A. Barth (2005), Coastal ocean response to summer upwelling favorable winds in a region of alongshore bottom topography variations off Oregon, *J. Geophys. Res.*, *110*, C10S04, doi:10.1029/2004JC002409.

Chan, F., J. A. Barth, J. Lubchenco, A. Kirincich, H. Weeks, W. T. Peterson, and B. A. Menge (2008), Emergence of anoxia in the California Current large marine ecosystem, *Science*, *319*, 920, doi:10.1126/science.1149016.

Connolly, T. P., B. M. Hickey, S. L. Geier, and W. P. Cochlan (2010), Processes influencing seasonal hypoxia in the northern California Current system, *J. Geophys. Res.*, *115*, C03021, doi:10.1029/2009JC005283.

Diaz, R. J., and J. Rosenberg (1995), Marine benthic hypoxia: A review of its ecological effects and the behavioural responses of benthic macrofauna, *Oceanogr. Mar. Biol.*, *33*, 245–303.

Erofeeva, S. Y., G. D. Egbert, and P. M. Kosro (2003), Tidal currents on the central Oregon shelf: Models, data, and assimilation, *J. Geophys. Res.*, *108*(C5), 3148, doi:10.1029/2002JC001615.

Grantham, B. A., F. Chan, K. J. Nielsen, D. S. Fox, J. A. Barth, A. Huyer, J. Lubchenco, and B. A. Menge (2004), Upwelling-driven nearshore hypoxia signals ecosystem and oceanographic changes in the Northeast Pacific, *Nature*, *429*, 749–754.

Gray, J. S., R. S. Wu, and Y. Y. Or (2002), Effects of hypoxia and organic enrichment on the marine environment, *Mar. Ecol. Prog. Ser.*, *238*, 249–279, doi:10.3354/meps238249.

Huyer, A., Sobey, E. J. C., and R. L. Smith (1979), The spring transition in currents over the Oregon continental shelf, *J. Geophys. Res.*, *84*, 6995–7011.

Keeling, R. F., A. Kortzinger, and N. Gruber (2010), Ocean deoxygenation in a warming world, *Annu. Rev. Mar. Sci.*, *2*, 199–229.

Kirincich, A. R., and J. A. Barth (2009), Along-shelf variability of inner-shelf circulation along the central Oregon coast during summer, *J. Phys. Oceanogr.*, *35*, 1380–1398, doi:10.1175/2008JPO3760.1.

Kirincich, A. R., J. A. Barth, B. A. Grantham, B. A. Menge, and J. Lubchenco (2005), Wind-driven inner-shelf circulation off central Oregon during summer, *J. Geophys. Res.*, *110*, C10S03, doi:10.1029/2004JC002611.

Kosro, P. M., W. T. Peterson, B. M. Hickey, R. K. Shearman, and S. D. Pierce (2006), Physical versus biological spring transition: 2005, *Geophys. Res. Lett.*, *33*, L22S03, doi:10.1029/2006GL027072.

Large, W. G., J. C. McWilliams, and S. C. Doney (1994), Oceanic vertical mixing: A review and a model with a nonlocal boundary layer parameterization, *Rev. Geophys.*, *32*, 363–403.

Nam, S. H., and U. Send (2011), Direct evidence of deep water intrusions onto the continental shelf via surging internal tides, *J. Geophys. Res.*, *116*, C05004, doi:10.1029/2010JC006692.

Nam, S. H., H. J. Kim, and U. Send (2011), Amplification of hypoxic and acidic events by La Niña conditions on the continental shelf off California, *Geophys. Res. Lett.*, *38*, L22602, doi:10.1029/2011GL049549.

Osborne, J. J., A. L. Kurapov, G. D. Egbert, and P. M. Kosro (2011), Spatial and temporal variability of the M2 internal tide generation and propagation on the Oregon shelf, *J. Phys. Oceanogr.*, *41*, 2037–2062. doi:10.1175/JPO-D-11-02.1.

Pawlowicz, R., B. Beardsley, and S. Lentz (2002), Classical tidal harmonic analysis including error estimates in MATLAB using T_TIDE, *Comput. Geosci.*, *28*, 929–937.

Pierce, S. P., J. A. Barth, R. E. Thomas, and G. W. Fleischer (2006), Anomalously warm July 2005 in the northern California Current: Historical context and significance of cumulative wind stress, *Geophys. Res. Lett.*, *33*, L22S04, doi:10.1029/2006GL027149.

Pierce, S. D., J. A. Barth, R. K. Shearman, A. Y. Erofeev (2012), Declining oxygen in the northeast pacific, *J. Phys. Oceanogr.*, *42*, 495–501. doi:10.1175/JPO-D-11–0170.1.

Reimers, C.E., H. T. Özkan-Haller, P. Berg, A. Devol, K. McCann-Grosvenor, and R. D. Sanders (2012), Benthic oxygen consumption rates during hypoxic conditions on the Oregon continental shelf: Evaluation of the eddy correlation method, *J. Geophys. Res. 117*, C02021, doi:10.1029/2011JC007564.

Schlax, M. G., and D. B. Chelton (1992), Frequency domain diagnostics for linear smoothers. *J. Am. Stat. Assoc.*, *87*, 1070–1081.

Send, U. and S. H. Nam (2012), Relaxation from upwelling: The effect on dissolved oxygen on the continental shelf, *J. Geophys. Res. 117*, C04024, doi:10.1029/2011JC007517.

Smith, R. L. (1981), A comparison of the structure and variability of the flow field in three coastal upwelling regions: Oregon, northwest Africa, and Peru, in *Coastal Upwelling, Coastal Estuarine Ser.*, vol. *1*, edited by F. A. Richards, pp. 107–118, AGU, Washington, D. C.

Steindler L., M. S. Schwalbach, D. P. Smith, F. Chan, and S. J. Giovannoni (2011), Energy starved candidatus pelagibacter ubique substitutes light-mediated ATP production for endogenous carbon respiration, *PLOS ONE 6*(5), e19725, doi:10.1371/journal.pone.0019725.

Suanda, A. and J. A. Barth (2012), Observations of high-frequency internal waves across the Oregon inner shelf, paper presented at 2012 Ocean Sciences Meeting, ASLO and AGU, Salt Lake City, Utah. [Available at http://www.sgmeet.com/osm2012/viewabstract2.asp?AbstractID=10085.]

Tengberg A., J. et al. (2006), Evaluation of a lifetime-based optode to measure oxygen in aquatic systems, *Limnol. Oceanogr. Methods*, *4*, 7–17.

Thomson, R. E., and M. V. Krassovski (2010), Poleward reach of the California undercurrent extension, *J. Geophys. Res.*, *115*, C09027, doi:10.1029/2010JC006280.

Whitney, F. A., H. J. Freeland, and M. Robert (2007), Persistently declining oxygen levels in the interior waters of the eastern subarctic Pacific, *Prog. Oceanogr.*, *75*, 179–199, doi:10.1016/j.pocean.2007.08.007.

Winant, C. D., R. C. Beardsley, and R. E. Davis, (1987), Moored wind, temperature, and current observations made during coastal ocean dynamics experiments 1 and 2 over the northern California continental shelf and upper slope, *J. Geophys. Res.*, *92*, 1569–1604.